The Orientational Influence on the Electronic Structure of the Solid fcc C_<60>

The Orientational Influence on the Electronic Structure of the Solid fcc C_{60} *

Bing-Lin Gu [a], [b], Yutaka Maruyama [a], Jing-Zhi Yu [a], Kaoru Ohno [a] and Yoshiyuki Kawazoe [a]

[a] *Institute for Materials Research, Tohoku University, Sendai 980, Japan*
[b] *Department of Physics, Tsinghua University, Beijing, 100084, China*

The comparison of the electronic structures of fcc C_{60} solids between two different molecular orientations has been done by performing a band structure calculation. We have found that the molecular orientation causes considerable changes on the degeneracies at Γ points, the dispersion of bands and the location of valence band maximum and conduction band minimum. The band variation upon molecular orientation should become an important subject in physics and materials science of the new class of solid fullerenes.

KEYWORDS: C_{60}, mixed-basis, electronic structure, orientation

1. Introduction

The success in efficiently synthesizing C_{60}[1],[2] has generated much interest in the chemical and physical properties of the new class of molecular crystals. The electronic and structural properties of the fullerites have been the subjects of numerous experimental and theoretical investigations.

Saito and Oshiyama[3] have calculated the cohesive property and band structure of face-centered-cubic(fcc) solid C_{60} crystal for the first time report, using the norm-conserving nonlocal pseudopotentials and a Gaussian orbital basis set. They found that, in fcc C_{60}, clusters are condensed by rather weak van der Waals force, and it is a semiconductor with direct energy gap of 1.5eV at the Brillouin-zone boundary X point, the width of the top valence band is 0.42eV. In their calculation, each fcc crystal axis crosses the double bond of molecule C_{60} at the midpoint.

Troullier and Martins[4] have also calculated the band structure of an fcc C_{60} using a "soft"pseudopotential local-density calculation with plane waves. Their results are quite different from the results of a local-density calculation with a Gaussian basis set; width of the top valence band is 0.58eV instead 0.42eV, and the gap is 1.18eV instead 1.5eV.

Recently, Shirley and Louie[5] have found the band gap of 2.15eV and about 1eV width for the HOMO and LUMO bands using a quasiparticle approach and suggested that the solid C_{60} is a standard band insulator.

As we know, a rapid rotation of $C_{60}(10^9/sec)$ in this crystal has already found to occur even at room temperature[6] and the C_{60} molecules are orientationally disordered and the crystal structure may be regarded as a face-centered cubic configuration. Below 260K, however, the molecules become orientationally ordered and simple cubic lattice results[7]−[10]. Moreover, the successful growth of oriented C_{60} fullerite layers on substrates has been reported[11]−[14]. Themlin et al.[11] have found the natural one-dimensional corrugation of the (001)

cleavage plane of GeS allows the growth of $C_{60}(111)$ fullerite layers. Hashizume et al.[12],[13] have observed firstly the different patterns of electronic partial charge densities of C_{60} layers deposited on Si(100) and Cu(111) surfaces.

From the above, it is clear that the band structure variation upon the orientation of C_{60} will become a very important subject in physics and materials science of the new class of solid fullerites.

This paper focuses on the effects of molecular orientation on electronic structure and charge distributions. Here we would like to treat the Fullerene molecules as accurate as possible because the effects depend on the fine structures in the crystal and should be considered in detail. Therefore, we have chosen a self-consistent mixed-basis full-potential approach within local density approximation(LDA).

The band structure calculation is carried out in the following two cases. First, we adopted the same orientation of the fullerene as that of Saito et al.[3] and Troullier et al.[4], i.e. the molecular unit is oriented in the highest possible symmetry T_h^3, as shown in Fig.1a. In this choice of the orientation of C_{60} molecule on fcc lattice sites, each molecule has twelve equivalent nearest-neighbor molecules, then, each pentagon in a C_{60} molecule has two C atoms which are nearest to the neighboring C_{60} molecule. In this case, our results agreed remarkably well with those of Troullier and Martins[4]. Second, we have placed the C_{60} molecule so that icosahedral axes are aligned with one of the crystallographic axis (see Fig.1b). We have found that this change in the orientation causes considerable change on the band structure of fcc C_{60}. Since the conduction band minimum occurs at L point in k-space and the valence band maximum at W point, the energy gap is changed to an indirect one. The degeneracies at the special k-points are also considerably released.

This paper is organized as follows. In Sec. 2, the method of the present calculation is described. In Sec. 3, the numerical results of band structure and charge distribution of fcc C_{60} are presented in two different cases,

and the influence of the rotation of the fullerenes on the electronic structures is reported. The conclusion is given in Sec. 4.
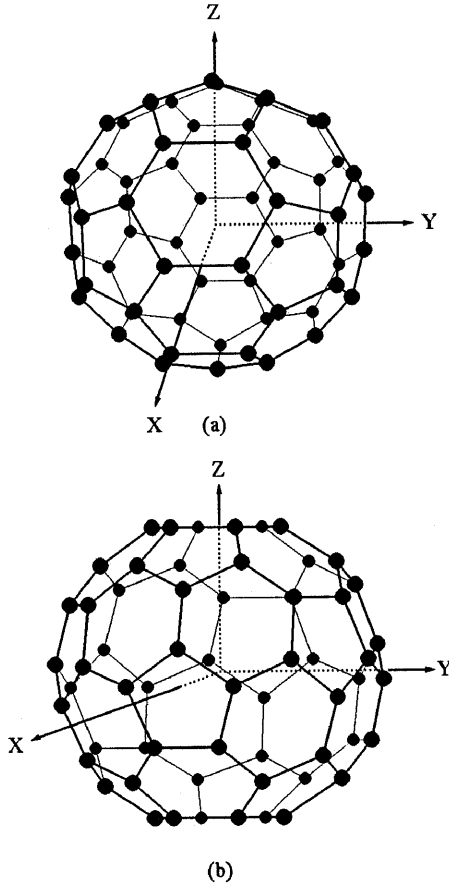

Figure 1. Atomic positions in the solid fcc C_{60}. (a) Each crystal axis crosses the double bond at the midpoint, this choice maintains the highest possible symmetry between the icosahedral symmetry of the C_{60} molecular units and the fcc lattice(Case 1); (b) One of the ten threefold icosahedral axes of C_{60} molecule is aligned with one of the crystallographic axis(Case 2).

2. Self-consistent mixed-basis full-potential approach

The mixed-basis method is first introduced by Louie et al.[15] for the calculation of the electronic structure of solids. A combined set of plane waves and Bloch sums of localized functions is employed as basis functions, thus leading to a very efficient representation of the system which contains both highly localized(atomic like) and delocalized(plane-wave-like) electrons.

Recently, we[16] have developed the mixed-basis method with full potential for the two-dimensional band structure calculation for the C_{60}'s on Si surface. In this case, the core states have been incorporated into the basis set, and the orthogonalization procedure is necessary.

The effective one electron Hamiltonian has the general form

$$H = T + V, \tag{1}$$

$$T = -\frac{1}{2}\nabla^2, \tag{2}$$

$$V(r) = -\sum_n \frac{Z_n}{|r - R_n|}$$

$$+ \int dr' \frac{\rho(r')}{|r - r'|} + V_{XC}(r), \tag{3}$$

where $V_{XC}(r)$ is a local exchange-correlation potential which is evaluated in the real space under local density approximation; in the X-α method, it is given by

$$V_{XC}(r) = -3\alpha(\frac{3}{8\pi}\rho(r))^{\frac{1}{3}}. \tag{4}$$

We used $\alpha = 0.7$ for this exchange-correlation parameter.

In the mixed-basis approach, for each k in the Brillouin zone, the basis set $|l\rangle$ consists of plane waves

$$\frac{1}{\sqrt{\Omega}}e^{i(k+K)\cdot r} \tag{5}$$

and Bloch sums of local orbitals

$$\Phi_{i\mu}(k,r) = \frac{1}{\sqrt{\Omega}}\sum_{R_m} e^{ik\cdot(R_m+\tau_i)}$$

$$\cdot f_{i\mu}(r - R_m - \tau_i), \tag{6}$$

where K is a reciprocal-lattice vector, R a primitive vector, τ_i a basis vector, μ a label for the orbitals on the ith atom, and Ω the crystal volume. In the present formulation, the localized functions $f_{i\mu}(r)$ which we call atomic orbitals, are chosen as: the damping parameter for 1s orbital, α, should not be confused with the exchange-correlation parameter in Eq.(4).

$$|1s\rangle = \sqrt{\frac{\alpha^3}{\pi}}e^{-\alpha|r-R_m-\tau_i|}, \tag{7}$$

$$|2p_x\rangle = \sqrt{\frac{\beta^5}{\pi}}(x - X_m - \tau_{ix})$$

$$\cdot e^{-\beta|r-R_m-\tau_i|}, \tag{8}$$

$$|2p_y\rangle = \sqrt{\frac{\beta^5}{\pi}}(y - Y_m - \tau_{iy})$$

$$\cdot e^{-\beta|r-R_m-\tau_i|}, \tag{9}$$

and

$$|2p_z\rangle = \sqrt{\frac{\beta^5}{\pi}}(z - Z_m - \tau_{iz})$$

$$\cdot e^{-\beta|r-R_m-\tau_i|}, \tag{10}$$

and the electron wave function is expressed by

$$\Psi_k(r) = \frac{1}{\sqrt{\Omega}}\sum_K A(k + K)e^{i(k+K)\cdot r}$$

$$+ \sum_{i\mu} \beta_{i\mu}(\mathbf{k})\Phi_{i\mu}(\mathbf{k,r}). \qquad (11)$$

Since the atomic wave functions are not orthogonal with plane waves, a modified equation which guarantees the orthogonality becomes

$$H\Psi_i = \epsilon_i S\Psi_i, \qquad (12)$$

where

$$S = \langle k|l \rangle \qquad (13)$$

is the overlap matrix of the wave functions. Introducing the lower half triangular matrix U which satisfies

$$S = UU^\dagger \qquad (14)$$

and introducing

$$U^\dagger\Psi_i = \Phi_i \qquad (15)$$

and

$$H' = U^{-1}HU^{\dagger -1}, \qquad (16)$$

we have

$$H'\Phi_i = \epsilon_i\Phi_i. \qquad (17)$$

To evaluate the charge density, one needs to trace the wave functions to those in the original nondiagonal form

$$\Psi_i = U^{\dagger -1}\Phi_i \qquad (18)$$

and

$$\rho(\mathbf{r}) = \sum_i^{occ} |\Psi_i|^2. \qquad (19)$$

In the calculation of the potential matrix element $\langle k|V|l \rangle$ and also the charge density $\rho(\mathbf{r})$, there are three types of combinations: (1) PW-PW, (2) PW-AO, and (3) AO-AO, where PW stands for plane-wave, and AO for atomic orbital. Because the 1s(core) and $2p_x$, $2p_y$, $2p_z$ atomic orbitals are well localized around each nucleus site, the combinations, PW-AO and AO-AO, are rather easily calculated straightforwardly in the real space, while for PW-PW the standard calculation in Fourier space is applied.

In the calculation of electronic structure of fcc C_{60}, we assume two C-C bond lengths in the C_{60} cage, i.e., 1.46Å on pentagons and 1.40Å on neighboring hexagons. The lattice constant is chosen to be $a=14.42$Å, so that the nearest neighbor distance of C_{60} molecule in fcc C_{60} is fit to the experimental value of 10.20Å.

As the basis set of each wave function, sixty 1s and sixty $2p_x$, sixty $2p_y$, sixty $2p_z$ atomic orbitals of C_{60}, and 2109 plane wave are adopted.

The exponential damping factor α and β for the 1s and 2p atomic orbitals are chosen as $\alpha = \frac{1}{0.106}$Å^{-1}, and $\beta = \frac{1}{0.133}$Å^{-1}, respectively.

The real space is divided into $64 \times 64 \times 64$ meshes, where 3.185 meshes correspond approximately to $1a.u. = 0.529$Å.
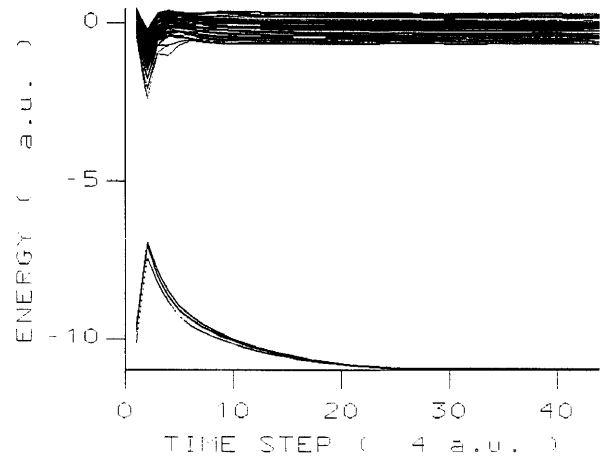

Figure 2. Variation of electronic energy level with the iteration step.

For the computation, we used NEC SX-3 supercomputer. The energies and wave functions of the electrons are obtained by the standard self-consistent iteration computation. Figure 2 shows the variation of electronic energy level as functions of the self-consistent iteration step. After 26 steps, all of the energy levels are well converged.

3. Results and discussion

We have calculated the band structure of fcc C_{60} in two different orientational cases.

Figure 3 shows the calculated HOMO and LUMO band structures for fcc-T_h^3 geometry corresponding to Case 1. As we know that the highest-occupied state of the C_{60} molecule has the h_u symmetry, this level is splitted by the tetrahedral crystal field into a t_u and an e_u states at Γ point and forms five dispersive bands. Both the valence-band maximum and conduction-band minimum are located at X point. The band gap is 1.10eV. The widths for HOMO(H_u), LUMO(T_{1u}) and next higher(T_{1g}) complexes of bands near the gap are 0.59, 0.59 and 0.56eV, respectively, exhibiting 30% enhancement of band widths as compared to the results by Saito-Oshiyama[3]. The present mixed-basis LDA results agree remarkably well with those of Troullier and Martins[4].

Figure 4 shows the calculated HOMO and LUMO band structures corresponding to Case 2. Our calculation with this case gives a typical example suggesting a strong influence of the rotation on the band structures in fcc C_{60}. We have found that the rotation causes considerable change on the band structure of fcc C_{60}. The highest-occupied state of the C_{60} molecule splits into two single states and a T_u state at Γ point, and both LUMO(T_{1u}) and next higher(T_{1g}) complexes of bands split into three single state at Γ point, respectively. The computed widths for the HOMO(H_u), LUMO(T_{1u}) and next higher(T_{1g}) complexes of bands near the gap are 0.6, 0.6 and 0.58eV, respectively, and the dispersions of the bands are broader than more symmetrical ones. Sur-
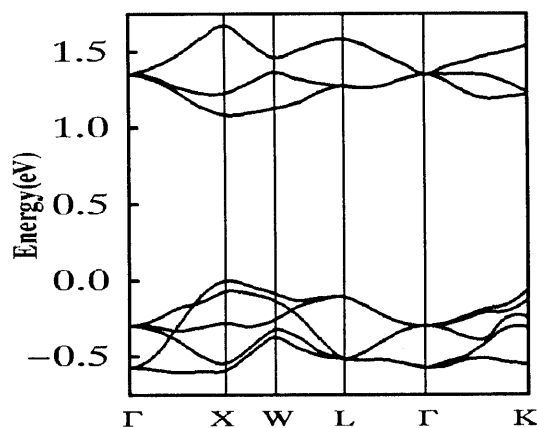
Figure 3. Calculated band structures for fcc-T_h^3 geometry corresponding to Case 1.
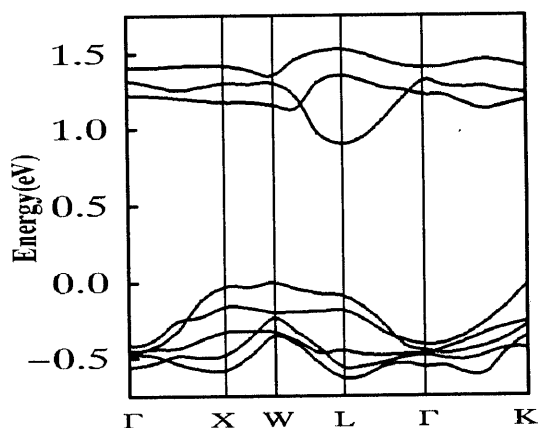

Figure 4. Calculated band structures corresponding to Case 2.

Figure 5. The spatial distributions of total charge density of fcc C_{60} inside the unit cell. (a) correspond to Case 1 and (b) to Case 2, respectively.

prisingly, the valence-band top moves to the W-point, and the conduction-band bottom moves to the L-point. The fcc C_{60} crystal becomes an indirect-gap semiconductor with an energy gap of 0.9eV.

Figure 5a and b indicate the spatial distributions of total charge densities of fcc C_{60} inside the unit cell corresponding to Case 1 and 2, respectively. There are net charge densities around the intermolecular region. In Case 2, there is even extra charge density in interstitial region. One can make the qualitative observation that the electronic distribution in Case 2 is not nearly so concentrated in the vicinity of the C-ion cores as it is in Case 1. As far as we know, appreciable overlap of atomic wave functions suggests the presence of broader bands. This is why the dispersions of bands corresponding to Case 2 are broader than those corresponding to Case 1.

To understand the split of energy level at Γ point, the charge density for 180th level is shown in Fig.6 on ⟨111⟩ direction. Regardless of the molecular orientations, within our choice, molecules form fcc lattice and have the same translational symmetry through Bravais lattice vectors. In general, however, molecules do not
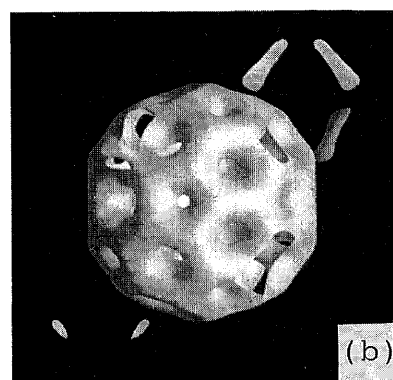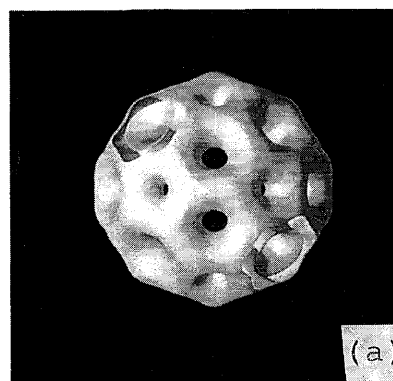
have the same point group symmetry due to different orientation in lattice. In Case 1 the wave function maintains the highest possible symmetry T_h^3, while in Case 2 the wave function symmetry becomes lower and it loses the degeneracies at special k-points.

We next show the spatial distribution of the partial charge density of HOMO(H_u) and LUMO(T_{1u}). Figure 7 is for the highest occupied valence orbitals(176-180th). It is clearly shown that most charge is located at the double bonds. There is a nonlocalized electronic cloud around interstitial region. In contrast to valence electron distribution, the electrons on the lowest unoccupied molecular orbitals (shown in Figure 8 for 181-183(T_{1u})) are located more at single bonds than double bonds and spread more and more as extended electronic cloud to interstitial region.

Troullier and Martins[4] have also given the charge density in contour plots of the wave function. The basic features are nearly the same as ours, especially for the lowest unoccupied molecular orbitals of C_{60}(Figure 8). The reliability of a method is limited not only by the accuracy of the computed solution to Schrödinger equation, which can be quite high, but also by the accuracy with which we have been able to estimate the potential V($\mathbf{r}$). Since Troullier et al. have used pseudopotential and we have used full-potential calculation, we believe our calculated results of charge density may be more
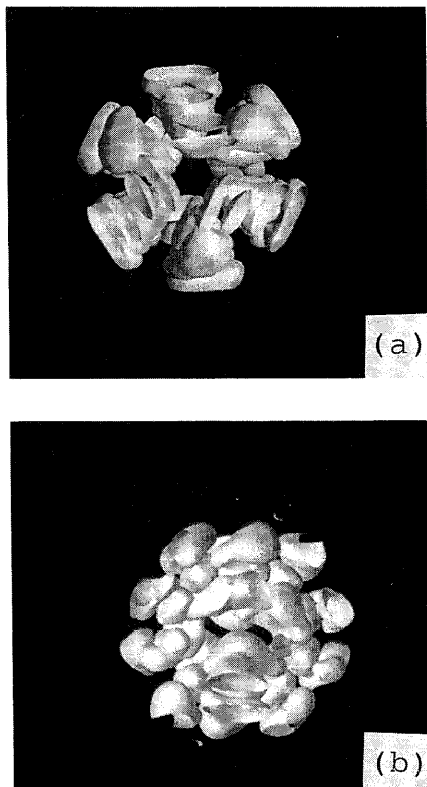
Figure 6. The charge density for the $180th$ level. (a) correspond to Case 1 and (b) to Case 2, respectively.

Figure 7. The spatial distributions of the sum of the highest occupied valence orbitals $(176 - 180th)$. (a) correspond to Case 1 and (b) to Case 2, respectively.

accurate than theirs.

It is very important to compare our theoretical calculation with the experimental results. Recently, the charge distribution can be accurately measured by scanning tunneling microscopy(STM). Hashizume et al.[13] have observed that bias voltage dependent STM images of individual C_{60} molecules show unique intramolecular structures. When the bias voltage is $V_b=-2.0V$, C_{60} molecular image appears in a doughnut shape, almost round with a hole at the center; when the bias voltage $V_b=2.0V$, an image with three fold symmetry appears evidently.

According to our calculation, the STM image at $V_b=-2.0V$ should correspond to the charge density of valence electron, the six-ring with three short bonds in doughnut shape should be observed(as shown in Figure 9a). On the contrary, the charge density of conduction electron should be observed at $V_b=2.0V$(as shown in Figure 9b). It is quite understandable when $V_b=-2.0V$, valence electron flows from C_{60} to tip; on the other hand, when $V_b=2.0V$, electron flows from tip to the conduction band of C_{60}.

4. Conclusion

We have investigated the effects of molecular orientation on the electronic structure of fcc C_{60} by performing a self-cons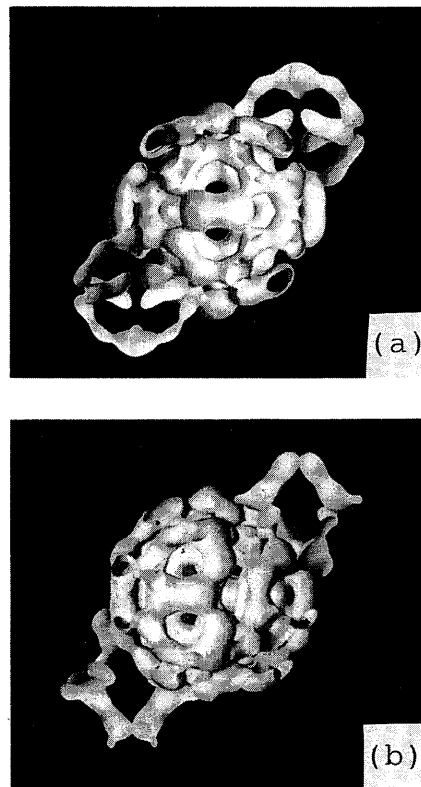istent mixed-basis full-potential band structure calculation within local density approximation for two different orientations of C_{60} in the fcc crystal. We have found that the orientation causes considerable change on the electronic structure of fcc C_{60}. At our selected two kinds of typical orientations, the degeneracies at Γ points for the highest occupied state split from $t_u + e_u$ into two single states and another T_u state, and both LUMO(T_{1u}) and next higher(T_{1g}) complexes of bands split from T_{1u} and T_{1g} into three single states, respectively. The dispersions of the bands are broader than the more symmetric one. Especially, the valence-band top moves from X-point to W-point and conduction band bottom moves to the L-point; the fcc C_{60} crystal becomes an indirect gap semiconductor with an energy gap of 0.9eV instead of the direct gap semiconductor with an energy gap of 1.1eV corresponding to the more symmetric one. The band variation upon rotation will become an important subject in physics and materials science of solid fullerenes.
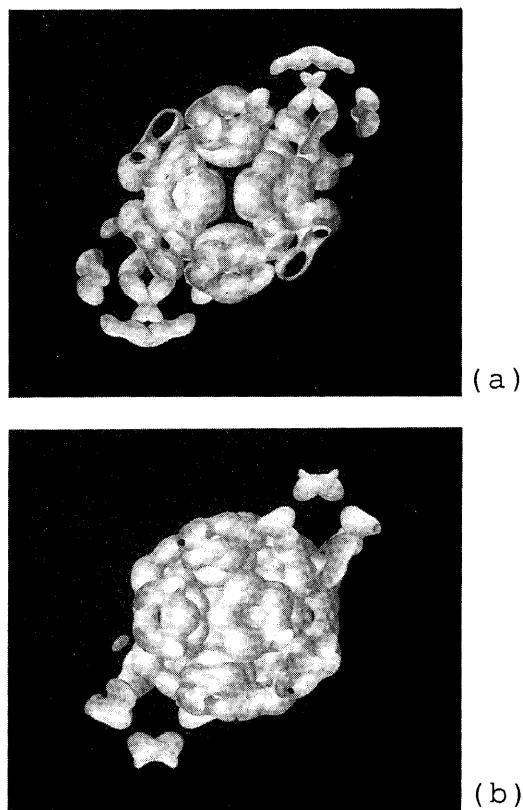
Figure 8. The spatial distributions of the sum of the lowest unoccupied conduction orbitals $(181 - 183th)$. (a) correspond to Case 1 and (b) to Case 2, respectively.
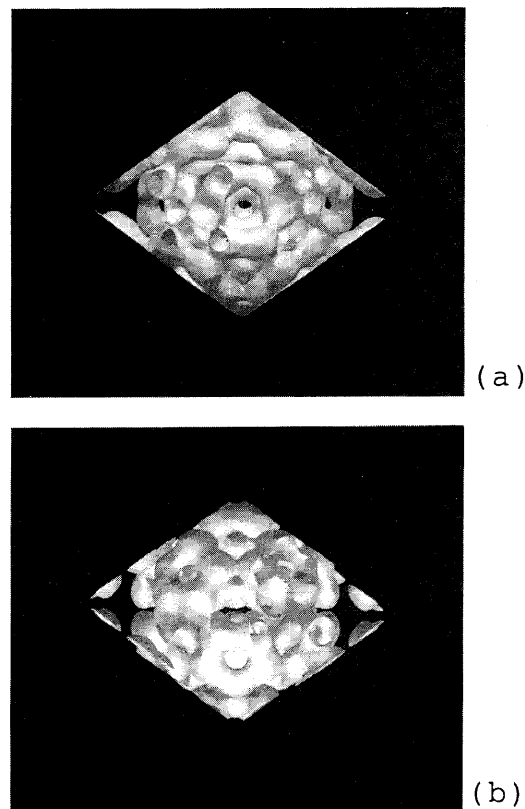
Figure 9. The partial charge distribution at the view of the (111) direction corresponding to Case 2. (a) valence band; (b) conduction band.

1) H. W. Kroto, J. R. Heath, S. C. O'Brien, R. E. Curl, and R. E. Smalley, Nature(London) **318**, 162(1985).

2) W. Krätschmer, L. D. Lamb, K. Fostiropocclos, and D. R. Hoffman, Nature(London) **347**, 354(1990).

3) S. Saito and A. Oshiyama, Phys. Rev. Lett. **66**, 2637(1991).

4) N. Troullier and José Luis Martins, Phys. Rev. B **46**, 1754(1992).

5) E. L. Shirley and S. G. Louie, Phys. Rev. Lett. 71(1), 133(1993)

6) C. S. Yannoni, J. Phys. Chem. **95**, 9(1991).

7) P. A. Heiney, J. E. Fishcher, A. R. McGhie, W. J. Romanow, A. M. Denenstein, J. P. McCauley, Jr., and A. B. Smith, III, Phys. Rev. Lett. **66**, 2911(1911).

8) R. Tycko, G. Dabbagh, R. M. Fleming, R. C. Haddon, A. V. Makkija, and S. M. Zahurak, Phys. Rev. Lett. **67**, 1886(1991).

9) W. I. F. David, R. M. Ibberson, J. C. Matthewman, K. Prassides, T. J. S. Dennis, J. P. Have, H. W. Kroto, R. Taylor, and D. R. M. Walton, Nature(London) **353**, 147(1991).

10) R. D. Johnson, C. S. Yannoni, H. C. Dorn, J. R. Salem, D. S. Bethune, Science **255**, 1235(1992).

11) J.-M. Themlin, S. Bouzidi, F. Coletti, J.-M. Debever, G. Gensterblum, Li-Ming Yu, J.-J. Pireaux, and P. A. Thiry, Phys. Rev. B **46**, 15602(1992).

12) T. Hashizume, X.-D. Wang, Y. Nishina, H. Shinohara, Y. Saito, Y. Kuk, and T. Sakurai, Jpn. J. Appl. Phys. **31**, L880(1992).

13) T. Hashizume, K. Motai, W.-D. Wang, N. Shinohara, Y. Saito Y. Maruyama, K. Ohno, Y. Kawazoe, Y. Nishina, H. W. Pickering, Y. Kuk, and T. Sakurai, Phys. Rev. Lett. 71(18), 2959(1993)

14) L. D. Lamb, D. R. Hoffman, R. K. Workman, S. Howells, T. Chen, D. Sarid, and R. F. Ziolo, Science **255**, 1413(1992).

15) S. G. Louie, K. M. Ho, and M. L. Cohen, Phys. Rev. B **19**, 1774(1979).

16) Y. Kawazoe, H. Kamiyama, Y. Maruyama, and K. Ohno, Jpn. J. Appl. Phys. **32**, 1433(1993).